Inelastic-neutron-scattering study of the Er^{3+} energy levels in $ErBa_2Cu_3O_7$

L. Soderholm, C.-K. Loong, and S. Kern
Argonne National Laboratory, Argonne, Illinois 60439
(Received 14 October 1991)

Magnetic excitation spectra of $ErBa_2Cu_3O_7$ have been measured by use of inelastic neutron scattering. Optimal experimental conditions allow the resolution of the transitions between the Er^{3+} ground state and all seven excited states within the $^4I_{15/2}$ Russell-Saunders ground multiplet. The data are analyzed in terms of an intermediate-coupling crystal-field model, calculated using spherical-tensor techniques. Calculated spectra based on the results of this analysis are consistent with all experimental spectra, including those obtained at higher temperatures. The eigenfunctions and eigenvalues obtained from this analysis are used to calculate the magnetic properties expected of Er^{3+} in this crystal environment.

INTRODUCTION

The high-T_c copper oxide superconductors are composed of two interpenetrating sublattices, either or both of which may be magnetic. One sublattice is composed of strongly covalent CuO sheets. The magnitude of the local copper moment and the cooperative behavior of the electrons (holes) in these sheets are strongly material dependent, primarily through details of oxygen stoichiometry.[1] Interactions between the electrons (holes) within these sheets are strong, as indicated by their high magnetic ordering or superconducting transition temperatures. The other sublattice may contain rare-earth ions (R), as, for example, in the $RBa_2Cu_3O_7$ compounds. In general, the f electrons of the rare-earth ions are more isolated from their surrounding environment than are the Cu d electrons. R usually possesses a large, local magnetic moment. The ionic character of the f-electron states remains intact except that the energy multiplets are split by the crystal field. The R moments do not couple strongly within the rare-earth sublattice, as indicated by their low magnetic ordering temperatures $T_N < 2.5$ K, with the exception of the Pr moments, which order at 17 K.[2] There also appears to be very little interaction between the local rare-earth moments and CuO sublattice; the size of the R moment does not influence the electronic behavior, such as the superconducting transition temperature T_c or the spin dynamics in the CuO planes.[1,3] The relative superconducting and magnetic interaction energies seen in these copper oxide systems are very different from previously studied magnetic superconductors, such as in binary intermetallics, where even minute concentrations of magnetic impurities strongly inhibit superconductivity. In ternary superconductors such as RRh_4B_4 or RMo_6S_8, the magnetic interactions between the two sublattices are comparable in energy to the superconducting interactions, leading to complex behavior in which the two types of ordering compete with each other.[4] In order to fully understand the magnetic properties of the rare-earth ions in superconducting oxides, it is necessary first to understand the electronic structure of the magnetic f states. The splitting of f states by a crystal field is normally modeled within the weak-field approximation; that is, the effects of electron-electron and spin-orbit coupling are considered large with respect to the crystal field.[5] We have successfully used this modeling scheme to account for the magnetic properties of trivalent R = Pr, Nd, and Ho in $RBa_2Cu_3O_7$. Since this work involves several rare-earth ions, it also provides a systematic understanding of the crystal-field splittings for all R in the $RBa_2Cu_3O_7$ environment.[6]

$ErBa_2Cu_3O_7$ is a 92-K superconductor, with only very weak, two-dimensional Er-Er magnetic interactions.[7] The intrinsic linewidths of the magnetic peaks are expected to be narrow, and the large, local moment on Er results in a good magnetic scattering cross section. Within the framework of model calculations for the $RBa_2Cu_3O_7$ series, we have predicted a splitting of the Er^{3+} ground term that is consistent with previous inelastic-neutron-scattering (NS) experiments,[8–10] although the data are not good enough to resolve the transitions at high energies. Our calculations show that transitions to all of the excited states within the ground multiplet should be observable, provided care is taken in the INS experiments to optimize resolution in the energy ranges of interest. With the predicted energy-level scheme as a guide, we have repeated the inelastic-neutron-scattering experiments. A preliminary account of this work is published elsewhere.[11] Here we report all the data as well as the detailed crystal-field analysis. The resulting crystal-field scheme is compared with our predictions and is then used to calculate the magnetic properties expected for Er in this environment.

EXPERIMENT

About 60 g of $ErBa_2Cu_3O_7$ were prepared by thoroughly mixing stoichiometric amount of Er_2O_3, $BaCO_3$, and CuO and firing the sample in air to about 950 °C. The sample was then reground and refired to about 980 °C under flowing oxygen and allowed to cool slowly. X-ray diffraction showed the sample to be single phase, and the orthorhombic unit cell constants refined to within acceptable values.

Inelastic-neutron-scattering experiments were per-

formed on polycrystalline materials using the high-resolution chopper spectrometer HRMECS at the Intense Pulsed Neutron Source (IPNS) of Argonne National Laboratory. Equipped with 100-K methane moderators, the Argonne pulsed spallation source provides a large flux of cold-to-epithermal neutrons that are essential to the study of magnetic excitations in rare-earth oxide superconductors. Using a two-rotor energy-selector system on HRMECS, crystal-field transitions at energies from 0.1 to 100 meV can be measured without disturbing the sample environment.

High resolution is required for measuring the fine splittings of the Er^{3+} crystal-field (CF) levels. The energy resolution ΔE [full width at half maximum (FWHM)] of the HRMECS spectrometer varies between 2% and 4% of the incident neutron energy (E_0) over the neutron-energy-loss region $E=E_0-E_1>0$ (where E_1 is the energy of the scattered neutron). Consequently, good resolution at an energy transfer E can be achieved by measurements chosen to maintain a small E_1. For example, when $E_0=4$ meV, $\Delta E\approx 0.12$ meV at $E=0.5$ meV, and when $E_0=110$ meV, $\Delta E\approx 2.5$ meV at $E=80$ meV. We have conducted INS experiments at 15, 80, 150, and 296 K with incident energies of 4, 8, 20, and 110 meV in order to cover the entire CF spectrum of the Er^{3+} ground term with good resolution. The $ErBa_2Cu_3O_7$ sample, contained in an aluminum planar cell, was mounted at a 45° angle to the incident beam. Such a geometry decreases the neutron traverse length in the sample to <5 mm for all detector angles (3°–140°), thereby reducing multiple-scattering effects. Background scattering was subtracted from the data by using empty-container runs. Measurements of elastic incoherent scattering from a vanadium standard provided detector calibration and intensity normalization.

The neutron-scattering cross section for crystal-field transitions in N noninteracting ions is given in the dipole approximation by

$$\frac{d^2\sigma}{d\Omega\, dE}=N\frac{\mathbf{k}_f}{\mathbf{k}_i}\frac{(\gamma r_0)^2}{4}g_J^2 S(\mathbf{Q},E)\ , \tag{1}$$

where the scattering function $S(Q,E)$ is expressed as

$$S(\mathbf{Q},E)=f^2(\mathbf{Q})e^{-2W(\mathbf{Q})}\times\sum_{n,m}\frac{\exp(-E_n/k_BT)}{Z}\times|\langle n|J_\perp|m\rangle|^2\delta(E_n-E_m-E)\ . \tag{2}$$

In the above equations, $\hbar\mathbf{Q}$ and E are the momentum and energy transfer, respectively, $\mathbf{k}_i$ ($\mathbf{k}_f$) is the initial (final) neutron wave vector, γ is the neutron magnetic moment in units of the nuclear Bohr magnetron, r_0 is the electron classical radius, g_J is the Landé g factor, $f(\mathbf{Q})$ is the ionic magnetic form factor, Z is the partition function, and $e^{-2W(\mathbf{Q})}$ is the Debye-Waller factor. In general, the ith CF state $|i\rangle$ at an energy E_i is a mixture of $|J,m\rangle$ states including those from higher J multiplets. $J_\perp$ is the component of the total angular momentum operator perpendicular to $\mathbf{Q}$. For experiments using polycrystalline samples and unpolarized neutrons,

$$|\langle|J_\perp|\rangle|^2=2(|\langle|J_x+J_y|\rangle|^2+|\langle|J_Z|\rangle|^2)/3\ ,$$

and only the modulus of $\mathbf{Q}$ is retained. Neutron-energy-loss processes correspond to the case $E=E_n-E_m>0$. At low temperatures these scattering processes dominate because the Boltzmann factors $\exp(-E_n/k_BT)$ are small except for the ground state. At elevated temperatures both neutron-energy-loss and -energy-gain ($E<0$) processes are seen in the measured spectra.

In general, the integrated intensity of a CF peak is proportional to the square of the matrix element for $J_\perp$ between two CF states. Therefore, by comparing the measured energies and intensities with a model calculation, the positions as well as the wave functions of the CF states can be identified unambiguously. Usually, the parameters used in the model are refined until good agreement between experiment and theory is reached and self-consistency is achieved throughout the redundant data.

The experimentally observed scattering cross section includes scattering of neutrons by magnetic electrons as well as by atomic nuclei. For polycrystalline samples nuclear scattering consists of an elastic peak at zero energy transfer and a diffuse background mainly due to phonon scattering. At small Q (<4 Å^{-1}) and at low temperatures, phonon contributions are small, and CF peaks can easily be identified. At larger Q or at elevated temperatures, phonon scattering usually dominates the measured spectrum. Thus studying the Q and temperature dependence of the measured intensities helps discern the origins of the scattering processes.

NEUTRON-SCATTERING RESULTS

It can be seen from Eqs. (1) and (2) that a transition between two CF levels will give rise to a peak in the observed neutron spectrum. The peak position corresponds to the energy separation of the levels, and the intrinsic width of the peak provides a measure of the finite lifetime of the two states involved in the transition. These lifetimes are influenced by interactions of the CF states with the surrounding environment. When the system is cooled to a temperature much lower than the first excited state, the only observable transitions are excitations from the ground state. In $ErBa_2Cu_3O_7$ the INS spectra at 15 K (well below the superconducting critical temperature of 91 K) provide clear evidence of seven magnetic transitions. Well-defined, sharp (resolution limited) CF peaks are observed at 9.2, 9.8, 11, 68, 72.5, 77, and 81 meV, as shown in Fig. 1. Since the $^4I_{15/2}$ Russell-Saunders ground multiplet of Er^{3+} is expected to be split into eight doubly degenerate levels, the 15-K spectra lead directly to the CF-level structure shown in Fig. 2. The observation of the three energy levels between 9 and 11 meV is consistent with some previously reported results.[8–10] The present experiment resolves four transitions in the E range of 68–81 meV, compared to the broad peak in the same region that has been previously interpreted as either one or two transitions.

As shown in Fig. 2, the Er^{3+} ground multiplet splits into two groups of CF states: four low-energy ($E\leq 11$

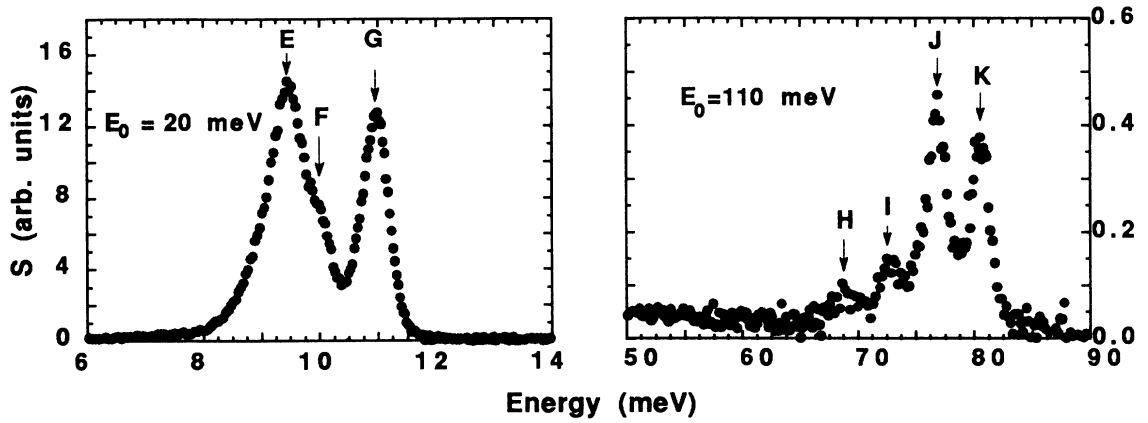

FIG. 1. Measured scattering functions of $ErBa_2Cu_3O_7$ at 15 K, obtained from inelastic-neutron-scattering measurements, with incident neutron energies of 20 meV (left) and 110 meV (right). Magnetic excitations from the crystal-field ground state to the seven excited doublet states within the $^4I_{15/2}$ multiplet are labeled alphabetically ($E-K$). The energy splitting scheme corresponding to these labels is shown schematically in Fig. 2.

meV = 128 K) doublets and four doublets in the 68–81-meV energy range. At a moderate temperature, say, 80 K, transitions occur from the thermally populated states to other states. Therefore INS measurements at higher temperatures provide useful confirmation of the energy-level scheme shown in Fig. 2. For example, Fig. 3 shows data obtained at 80 K, with incident energies of 4 and 8 meV. The peaks at ± 1.2 meV (labeled C and A) are assigned to the transitions between the energy levels at 9.8 and 11 meV, while the peak at 0.6 meV (labeled B) corresponds to a transition between 9.2 and 9.8 meV (see also Fig. 2). The peak at 1.8 meV, labeled D in Fig. 3(b), corresponds to transition from the 9.2-meV state to the 11-meV state. The data obtained at 150 K with an incident neutron energy of 110 meV are shown in Fig. 4. The peaks observed at 68, 72, 77, and 81 meV have decreased in intensity relative to the 15-K data, while there are several overlapping additional peaks corresponding to CF transitions from the lower excited states to the high-energy states. At least three new peaks at 59, 62, and 66 meV, labeled L, M, and N, respectively, in Fig. 4 are well

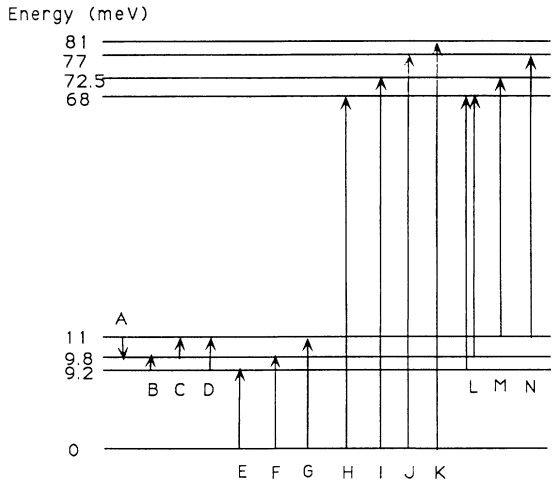

FIG. 2. Schematic diagram of the splitting of the $^4I_{15/2}$ Russell-Saunders ground multiplet, determined by neutron-scattering experiments. The transitions labels refer to the experimentally resolved transitions shown in Figs. 1, 3, and 4.

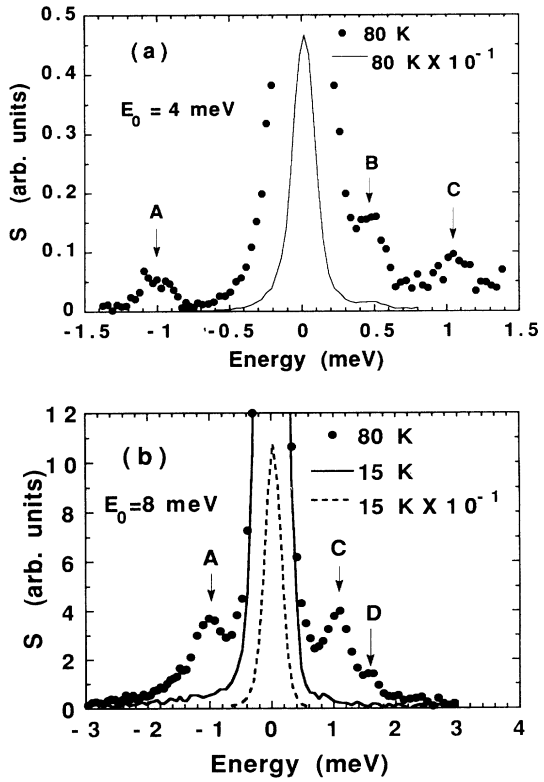

FIG. 3. Measured scattering functions of $ErBa_2Cu_3O_7$ at 80 K with $E_0=4$ meV (a) and at 80 and 15 K with $E_0=8$ meV (b). The peaks (A through D) correspond to crystal-field transitions between thermally occupied excited states, which are observable only at elevated temperatures (80 K) (see also Fig. 2).

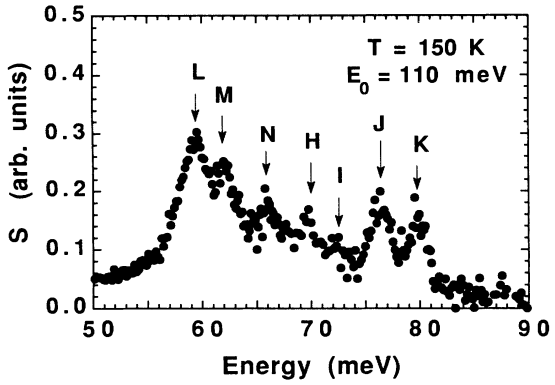

FIG. 4. Measured scattering functions of $ErBa_2Cu_3O_7$ at 150 K. The labeled crystal-field peaks correspond to the resolved transitions shown in Fig. 2. The broad background over the entire energy range consists of other overlapping crystal-field transitions and phonon scattering.

resolved. They correspond to those transitions shown in Fig. 2. In addition, the CF peaks at high temperatures have larger widths, indicating stronger relaxation effects due to interactions with other excitations such as phonons. Strong coupling of phonons and a CF state at about 37 meV in $NdBa_2Cu_3O_7$ have been reported in a recent Raman-scattering study.[12] Coupling of phonons to CF excitations in general depends on the energies and symmetries of individual vibrational modes and CF states. In $ErBa_2Cu_3O_7$ all the observed CF peaks at 15 K have widths comparable to instrumental resolution, indicating that interactions between CF excitations and phonons are weak. However, the present INS measurements using a polycrystalline sample are probably not sensitive enough to detect subtle effects of specific CF-phonon coupling.

CRYSTAL-FIELD ANALYSIS

The data described above are sufficient to allow the refinement of crystal-field parameters appropriate to Er^{3+} in paramagnetic $ErBa_2Cu_3O_7$. The method used here for fitting the energy levels and calculating the magnetic properties of the $4f^{11}$ configuration of Er^{3+} in a crystal field was developed by Crosswhite and Crosswhite.[13] All of the interactions included in the model are diagonalized simultaneously. For convenience, the total Hamiltonian is considered to consist of two parts:

$$H = H_{\mathrm{FI}} + H_{\mathrm{CF}} .$$

Here H_{FI} is the free-ion contribution, which includes the spherically symmetric, one-electron term of the Hamiltonian, the electrostatic interaction between equivalent f electrons, the spin-orbit interaction, and a term accounting for higher-order corrections.[14] H_{CF} is the crystal-field term, which incorporates the effects of the electrostatic interactions arising from the surrounding charges on the f electrons of a single ion. The crystal-field part of the Hamiltonian is written

$$H_{\mathrm{CF}} = \sum_{k,q,i} B_q^k C_q^k(i) ,$$

where $C_q^k(i)$ is a spherical tensor of rank k, dependent on the coordinates of the ith electron, the summation of i is over all f electrons of the ion, and B_q^k are the crystal-field coefficients. The site symmetry of the ion of interest determines which B_q^k parameters are nonzero.

The full Hamiltonian described above is diagonalized, using as the basis functions the 100 lowest-energy states of an f^{11} configuration (i.e., the eigenstates of the free-ion Hamiltonian). The free-ion contribution to the total Hamiltonian is characterized by a set of parameters obtained for $Er:LaF_3$.[14] The choice of free-ion parameters does not significantly influence our results, since the first excited J multiplet is at high energy (≈ 800 meV) relative to the splittings within the ground multiplet (≈ 80 meV). In fact, contributions from the higher-energy Russell-Saunders multiplets are often ignored in the treatment of lower-energy data such as that under consideration here, allowing for the use of much simpler formalisms, such as that developed by Stevens.[15] Although this simplification works well for the heavier lanthanides, including Er^{3+}, we employ the more complete treatment for consistency with our other work on the lighter lanthanides.[16] Conversion of the crystal-field parameters listed here to those of Stevens, as outlined by Kassman,[17] results in parameters which provide essentially similar energies and eigenvalues.

The site symmetry of the rare earths in the $RBa_2Cu_3O_7$ orthorhombic structure is the mmm (D_{2h}) point group,[18] so the crystal field is characterized by nine real B_q^k parameters. In principle, a site of this symmetry will split the Er^{3+} Russell-Saunders ground multiplet ($^4I_{15/2}$) into eight doublets, and therefore at low temperatures there are a maximum of seven magnetic transitions expected between the ground and accessible excited states, which are all within the ground multiplet.

As summarized in Fig. 2, we observe all seven possible transitions from the ground state. While these observations make the energy-level assignments unambiguous, the limited data available to fit nine independent crystal-field parameters (i.e., seven energy levels and seven transition intensities) necessitate a judicious choice of starting parameters. Since there are so few data, the fit obtained may depend on the input starting parameters, and care must be taken in their choice.

As can be seen from Fig. 5, the site symmetry of the rare earths in the lattice under study is only slightly distorted from cubic. A comparison of the energy splittings observed experimentally with those expected for Er^{3+} in a cubic field reveals a close correspondence. The use of a purely cubic field as a starting assumption greatly simplifies the problem because there are only two independent parameters, one fourth and one sixth order. We have taken advantage of this correspondence by beginning our analysis with cubic symmetry and then descending in symmetry first to tetragonal and finally to true orthorhombic symmetry. The progression of the energy-level splittings with descent in symmetry is shown in Fig. 6.

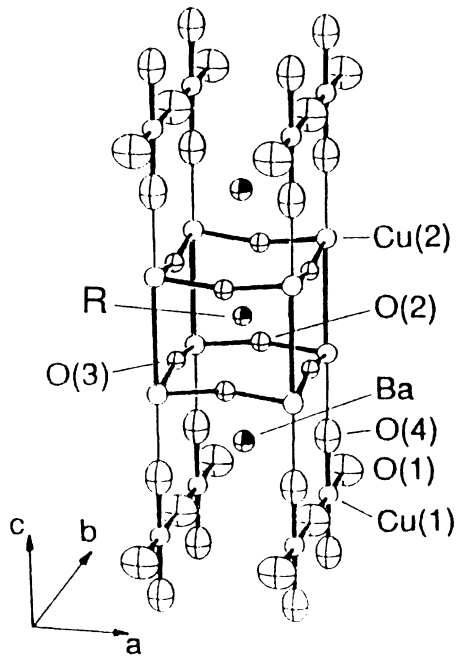

FIG. 5. Crystal structure of $R\mathrm{Ba_2Cu_3O_7}$ (Ref. 18), demonstrating the environment of the rare-earth ion.

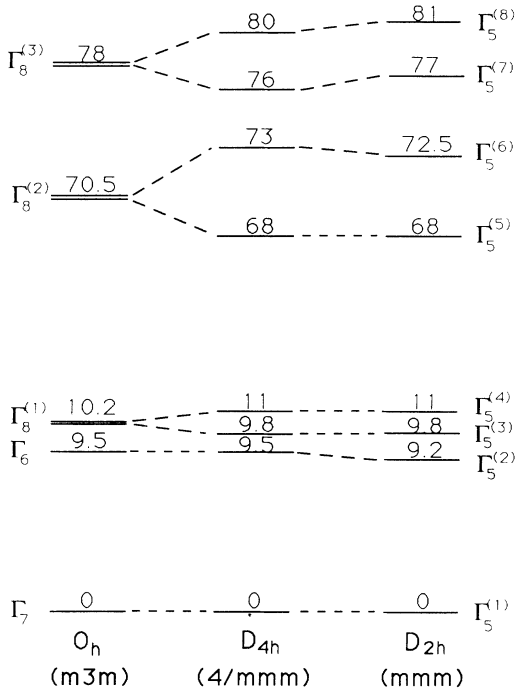

FIG. 6. Calculated crystal-field-level schemes for Er^{3+} ions in $\mathrm{ErBa_2Cu_3O_7}$, as the symmetry at R descends from cubic to tetragonal to orthorhombic. The energies are in units of meV.

Using the formalism developed by Lea, Leask, and Wolf, we find a ratio of fourth- to sixth-order parameters of ≈ -0.4 (Ref. 19) (with B's in the Stevens notation), which provides us with a direct estimate of the B_0^4, B_4^4, B_0^6, and B_4^6 parameters. Using these parameters and cubic constraints, we fitted the data to obtain the parameters listed in Table I as the cubic parameters.

With a good estimate of starting values for the cubic parameters, we look for estimates of the contributions arising from the lower symmetry of the R site. We obtain these from a superposition model,[20] as described by Nekvasil.[21] The cubic crystal-field values obtained by this modeling procedure agree in sign and magnitude with our fitted values. As shown in Table I, the superposition model gives a prediction of the sign and magnitude of the fourth- and sixth-order noncubic terms. Unfortunately, the superposition model does not work well for second-order parameters.[20]

Second-order crystal-field parameters are often the hardest to estimate. Fortunately, these parameters can be calculated from available ^{155}Gd Mössbauer data.[22–25] The only contribution to the measured electric-field gradient at the Gd nucleus is from the lattice, since the $4f$-electron density is spherically symmetric to first order. Using the experimentally determined values of the electric-field gradient, $e^2qQ = -230$ MHz, and the gradient assymmetry parameter $\eta = 0.4$, we obtain the B_0^2 and B_2^2 parameters, applicable to Er, which are listed in Table I.

For comparison, Table I also lists the crystal-field B_q^k's which are scaled from our previous work on Pr, Nd, and Ho.[16] Scaling crystal-field parameters obtained for Ho in $R\mathrm{Ba_2Cu_3O_7}$ (Refs. 16 and 26) to appropriate parameters for Nd and Pr has provided us with scaling laws which can be used to predict parameters for other R in this site.[6] The overall scaling is accomplished by adjusting the B's by relative values of $\alpha\langle r^n\rangle_{\mathrm{HF}}$, where $\alpha \approx 0.6$ for all n (Ref. 27) and $\langle r^n\rangle_{\mathrm{HF}}$ are the calculated free-ion Hartree-Fock radial parameters of the nth order.[28] In this way a consistent set of starting parameters can be obtained for all R in $R\mathrm{Ba_2Cu_3O_7}$.[6] The starting parameters appropriate to Er are shown in Table I as the "Scaled" parameters.

The signs and magnitudes of most of the estimated parameters agree very well, the most notable differences being the B_2^4 and B_2^6 values calculated from the superposition and scaling models. Together with B_2^2 and B_6^6, these are the four extra parameters that must be included when descending in site symmetry from $4/mmm$ (D_{4h}) to mmm (D_{2h}). $4/mmm$ is the site symmetry of the rare earth in the tetragonal form of $R\mathrm{Ba_2Cu_3O_7}$.[29] As shown in Fig. 5, the distortion of the Er near neighbors from $4/mmm$ to mmm site symmetry is very small; therefore the superposition model is not expected to predict accurately these added parameters. Although they are small, crystal-field energy levels are sensitive to these parameters, particularly B_2^2 and B_2^4. Small changes in these values cause notable changes in the multiplet of states calculated near 10 meV. A sensitivity to the transition energies and intensities to changes in oxygen content (and therefore symmetry) has also been observed experimentally.[30]

We used our cubic parameters (releasing their con-

TABLE I. Crystal-field parameters, originating from different sources, used for calculating the energy-level splittings of Er^{3+} in $ErBa_2Cu_3O_7$. Values listed are those obtained by (a) fitting the data assuming cubic symmetry, (b) calculated from a superposition (SP) model (Ref. 21), (c) analyzing the electric-field gradient obtained from ^{155}Gd Mössbauer spectroscopy in terms of the lattice, second-order crystal-field parameters (Refs. 22–25), and (d) scaling parameters previously obtained by fitting INS data on Pr, Nd, and Ho (Scaled) (Ref. 16). The last column lists our best-fit parameters assuming *mmm* site symmetry. All parameters are in units of cm^{-1}.

	Cubic fit	SP	Mössbauer	Scaled	Final fit
B_0^2			350	431	324
B_2^2			56	60	150
B_0^4	−2090	−1852		−1794	−1942
B_2^4		123		−336	−4
B_4^4	1249	1039		977	1338
B_0^6	612	595		429	458
B_2^6		−1		−243	−56
B_4^6	1145	1254		1170	1237
B_6^6		2		−15	0[a]

[a]Simulations show the system to be insensitive to this parameter; therefore it was fixed at zero for all fits.

straints), the superposition parameters, and the Mössbauer second-order parameters as starting values for our fit. The fits were insensitive to the magnitude of B_6^6; therefore it was fixed at zero. We obtained the final set of crystal-field parameters listed in Table I and the energy levels and transition-matrix elements listed in Table II. The calculated spectra obtained from these parameters agree well with both the energies and intensities of the peaks. Selected calculated spectra are shown in Fig. 7. In particular, the similarity of the experiment and calculated spectra at 150 K should be noted. The magnitude of the fitted parameters clearly reflects the predominantly cubic symmetry of the site. The parameters introduced in the descent to *4/mmm* site symmetry are much smaller, and the parameters necessary to further reduce the symmetry to *mmm* are the smallest. While the data can be approximately represented by tetragonal symmetry, a good fit to both the observed energies and intensities requires the complete *mmm* symmetry. The good agreement between our final parameters and those obtained from appropriately scaling our previously determined values for Ho, Nd, and Pr shows that our scaling procedure is effective in transferring parameters from one R to another. Perhaps even more importantly, these results strongly support our parametrization of the crystal field at the rare-earth site.

MAGNETIC PROPERTIES

The fitting of a crystal-field scheme to experimental data enables the calculation of a variety of other properties using the eigenfunctions and eigenvalues obtained from the crystal-field analysis. Experiments have shown that $ErBa_2Cu_3O_7$ is a Curie-Weiss paramagnet down to low temperatures. The value of the effective magnet moment, determined over the temperature range of about 50–300 K, is somewhat sample dependent, but in the range $9.6–9.95\mu_B$.[1] At much lower temperatures (i.e., ≤ 1 K, the system shows evidence of two-dimensional (2D) ordering in the a-b plane, with a transition to 3D long-range order at about 600 mK.[7] The saturation moment (μ_{sat}) associated with this ordered state was determined by neutron diffraction to be $4.8(2)\mu_B$.[31]

The paramagnetic susceptibility expected for the Er sublattice can be calculated using the van Vleck formalism:[32,33]

$$\chi=\frac{N\mu_B^2}{3k_BTZ}\sum_{n,i}\left[\sum_j|\langle\phi_{n,i}|\mu|\phi_{n,j}\rangle|^2-2\sum_{j,m\neq n}\frac{|\langle\phi_{n,i}|\mu|\phi_{m,j}\rangle|^2}{E_n-E_m}k_BT\right]\times\exp\left[\frac{-E_n}{k_BT}\right],$$

where $Z=\sum_n d_n\exp(-E_n/k_BT)$. Here ϕ_{nl} are the d_n degenerate eigenfunctions with energy E_n in the absence

TABLE II. Observed energy levels of Er^{3+} in $ErBa^2Cu_3O_7$ compared with those obtained from the crystal-field B_q^k values listed in Table I. These energy levels are all doubly degenerate, and all have the symmetry classification Γ_5 in a site with orthorhombic symmetry. The calculated magnetic transition strengths at zero energy correspond to elastic scattering within the ground doublet. Those at nonzero energies correspond to transitions from the ground state to each excited state.

Observed E (meV)	Calculated E (meV)	Magnetic transition $\mu_\parallel^2$	Strength (μ_B^2) $\mu_\perp^2$
0	−0.38	4.903	15.539
9.4	9.4	12.822	2.905
9.8	10.0	3.953	3.207
11	11.0	0.005	8.573
67.5	67.3	0.169	0.186
72.5	72.4	0.031	0.654
77	77.1	0.176	1.607
81	80.7	2.753	0.694

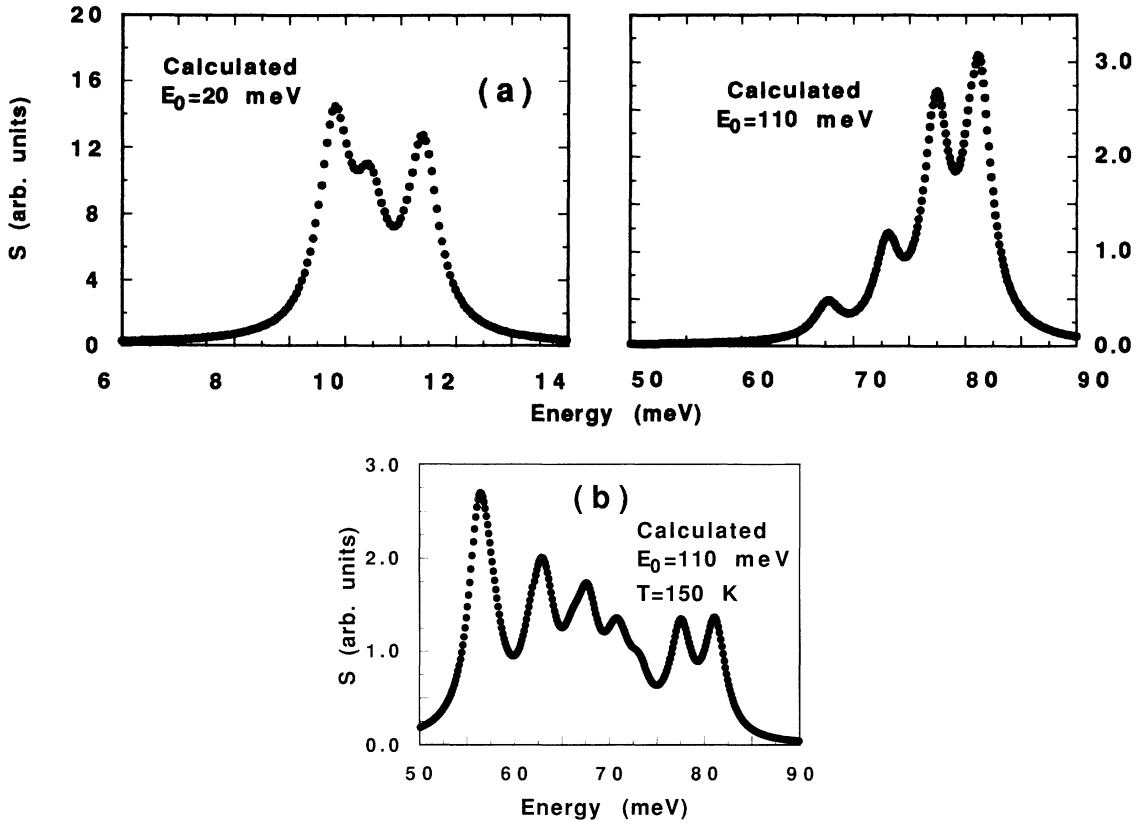

FIG. 7. Calculated magnetic scattering functions of $ErBa_2Cu_3O_7$ using the final crystal-field parameters (see Table I): (a) $T=15$ K and (b) $T=150$ K. Effects of instrumental resolution and the Q dependence of the Er^{3+} magnetic form factor have been taken into account in the calculation.

of a magnetic field. The magnetic-moment operator is $\mu=\mathbf{L}+2\mathbf{S}$. The perpendicular and parallel susceptibilities (relative to the crystal-field principal axis) calculated in this manner are shown as a function of temperature in Fig. 8. There is a small anisotropy predicted for the susceptibilities at low temperature. The effective moment obtained by fitting to a Curie law the calculated data in the temperature range 50–300 K (see inset Fig. 8) is $9.53\mu_B$, which is very close to the effective moment of $9.58\mu_B$ expected for a Er^{3+} free ion. The measured effective moment for $ErBa_2Cu_3O_x$ is reported as $9.93\mu_B$ for $x\approx 6.8$ or $9.63\mu_B$ for $x\approx 6.2$.[1] The larger value of the measured moment over the Er^{3+} free-ion value is most probably due to a contribution from the copper sublattice, which is expected to be sample dependent and somewhere in the range of $(0-0.4)\mu_B$.[34]

In addition to the magnetic susceptibility, the ground-state saturation moment can be estimated by including the molecular field (H_m) as a perturbation to the crystal field. The magnitude of the molecular field can be estimated from[35]

$$T_N=g_J(\langle J_Z\rangle+1)\mu_B H_m/3k_B\ ,$$

where g_J is the Landé factor, H_m is the molecular field at the Er site, k_B is the Boltzmann constant, and the 3D magnetic ordering temperature $T_N=600$ mK.[7] Using the molecular field determined in this way, the saturation moment ($\mu_{\rm sat}$) can be calculated. It turns out that the magnitude of the saturation moment is relatively insensitive to the magnitude of the molecular field, justifying the use of an estimate based on an oversimplified molecular-

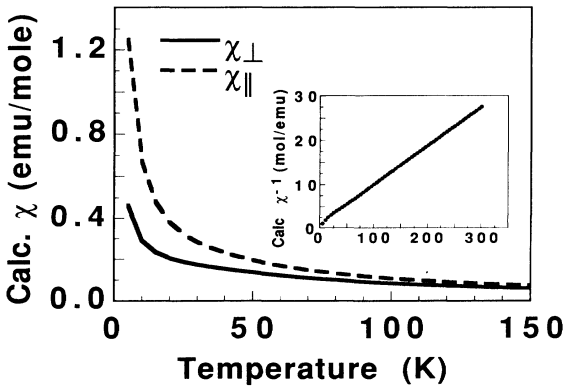

FIG. 8. Paramagnetic susceptibility of $ErBa_2Cu_3O_7$ using the final crystal-field-level scheme. $\chi_\perp$ and $\chi_\parallel$ are components of the susceptibility perpendicular to and parallel with the crystallographic c direction, respectively. The inset shows the averaged inverse magnetic susceptibility vs temperature.

field expression. Calculations performed with the molecular-field direction parallel to the principal crystal-field axis, produce a $\mu_{sat}=1.4\mu_B$, while a value of $\mu_{sat}=3.4\mu_B$ is obtained when the molecular-field direction is perpendicular to the principal axis. We know from previous work[36] that the principal axis of the crystal-field tensor is coincident with the crystallographic c direction; therefore we can relate our calculated moments to experiment. The relative energies of the Kramers states, split by applied field, are calculated with the moment in the a-b plane or parallel to the c axis. The magnitude of the splittings is the same, to within the estimated error of the calculation, so that an ordered moment direction cannot be determined directly by applying a molecular field to the calculated wave functions. Our calculated moment of $3.4\mu_B$ is only in fair agreement with the experimental result of $4.8\mu_B$.[31]

CONCLUSIONS

A combination of predictive capabilities and recent INS instrument upgrades permits the unambiguous determination of the eight crystal-field states of the Er^{3+} $^4H_{15/2}$ Russell-Saunders ground multiplet. Estimates of the crystal-field parameters necessary to fit these INS data are obtained from several sources and provide good starting parameters for the data analysis. The transition energies and intensities are well represented by values calculated with the best-fit parameters. The good agreement between our fitted parameters and those obtained by scaling our previous results on Ho, Nd, and Pr shows that we have successfully represented the crystal field at R by this parametrization. The eigenfunctions and eigenvalues from this analysis are used to calculate the contribution of the Er^{3+} ion to the total magnetic susceptibility of $ErBa_2Cu_3O_7$ and also the saturation moment expected at low temperature in the magnetically ordered state.

ACKNOWLEDGMENTS

This work is supported by the U.S. DOE, Basic Energy Sciences, and has benefited from the use of the Intense Pulsed Neutron Source at Argonne National Laboratory, all under Contract No. W-31-109-ENG-38.

[1]J. M. Tarascon, W. R. McKinnon, L. H. Greene, G. W. Hull, and E. M. Vogel, Phys. Rev. B **36**, 226 (1987).
[2]A review is given in *High Temperature Superconductivity,* edited by J. W. Lynn (Springer, New York, 1989).
[3]L. F. Schneemeyer, J. V. Waszczak, S. M. Zahorak, R. B. vanDover, and T. Seigrist, Mater. Res. Bull. **22**, 1467 (1987).
[4]For a review, see *Superconductivity in Ternary Compounds,* Vols. 32 and 34 of *Topics in Current Physics,* edited by O. Fischer and M. B. Maple (Springer, New York, 1982).
[5]Brian G. Wybourne, *Spectroscopic Properties of Rare Earths* (Interscience, New York, 1965), p. 236.
[6]L. Soderholm and C.-K. Loong (unpublished).
[7]J. W. Lynn, T. W. Clinton, W.-H. Li, R. W. Erwin, J. Z. Liu, K. Vandervoort, and R. N. Shelton, Phys. Rev. Lett. **63**, 2606 (1989).
[8]U. Walter, S. Fahy, A. Zettl, Steven G. Louie, Marvin L. Cohen, P. Tejedor, and A. M. Stacey, Phys. Rev. B **36**, 8899 (1987).
[9]P. Allenspach, A. Furrer, B. Rupp, and H. Blank, Physica C **161**, 671 (1989).
[10]P. Allenspach, A. Furrer, J. Mesot, U. Staub, H. Blank, H. Mutka, C. Vettier, E. Kaldis, J. Karpinski, S. Rusiecki, and A. Mirmelstein (unpublished).
[11]L. Soderholm, C.-K. Loong, and S. Kern, J. Less-Common Met. (to be published).
[12]E. T. Heyen, R. Wegerer, and M. Cardona, Phys. Rev. Lett. **67**, 144 (1991).
[13]H. M. Crosswhite and H. Crosswhite, J. Opt. Soc. Am. B **1**, 246 (1984).
[14]W. T. Carnall, G. L. Goodman, K. Rajank, and R. S. Rana, J. Chem. Phys. **90**, 3443 (1989).
[15]K. W. H. Stevens, Proc. Phys. Soc. London A **65**, 209 (1952).
[16]L. Soderholm, C.-K. Loong, and G. L. Goodman, Phys. Rev. B **43**, 7923 (1991).
[17]A. J. Kassman, J. Chem. Phys. **53**, 4118 (1970).
[18]M. A. Beno, L. Soderholm, D. W. Capone II, D. G. Hinks, J. D. Jorgensen, Ivan K. Schuller, C. U. Segre, K. Zhang, and J. D. Grace, Appl. Phys. Lett. **51**, 57 (1987).
[19]K. R. Lea, M. J. M. Leask, and W. P. Wolf, J. Phys. Chem. Solids **23**, 1381 (1962).
[20]D. J. Newman and Betty Ng, Rep. Prog. Phys. **52**, 699 (1989).
[21]V. Nekvasil, Solid State Commun. **65**, 1103 (1988).
[22]E. E. Alp, L. Soderholm, G. K. Shenoy, D. G. Hinks, D. W. Capone II, K. Zhang, and B. D. Dunlap, Phys. Rev. B **36**, 8910 (1987).
[23]G. Wortmann, C. T. Simmons, and G. Kaindl, Solid State Commun. **64**, 1057 (1987).
[24]H. H. A. Smit, M. W. Dirken, R. C. Thiel, and L. J. deJongh, Solid State Commun. **64**, 695 (1987).
[25]S. Ofer, I. Nowik, and S. G. Cohen, in *Chemical Applications of Mossbauer Spectroscopy,* edited by, V. I. Goldanskii and R. H. Herber (Academic, New York, 1968), pp. 488–503.
[26]A. Furrer, P. Bruesch, and P. Unternahrer, Phys. Rev. B. **38**, 4616 (1988).
[27]G. L. Goodman, C.-K. Loong, and L. Soderholm, J. Phys. Condens. Matter **3**, 49 (1991).
[28]A. J. Freeman and R. E. Watson, Phys. Rev. **127**, 2058 (1962).
[29]J. D. Jorgensen, M. A. Beno, D. G. Hinks, L. Soderholm, K. J. Volin, R. L. Hitterman, J. D. Grace, and Ivan K. Schuller, Phys. Rev. B **36**, 3608 (1987).
[30]Albert Furrer and Peter Allenspach, J. Phys. Condens. Matter **1**, 3715 (1989).
[31]T. Chattopadhyay, P. J. Brown, B. C. Sales, L. A. Boatner, H. A. Mook, and H. Maletta, Phys. Rev. B **40**, 2624 (1989).
[32]J. H. van Vleck, *The Theory of Electric and Magnetic Susceptibilities* (Oxford University Press, London, 1932).
[33]R. M. White, *Quantum Theory of Magnetism,* Springer Series in Solid-State Sciences, Vol. 32 (Springer, New York, 1983).

[34]D. C. Johnston, S. K. Sinha, A. J. Jacobson, and J. M. Newsam, Physica C **153-155**, 572 (1988).
[35]B. D. Cullity, *Introduction to Magnetic Materials* (Addison Wesley, Reading, MA, 1972).
[36]P. Allenspach, A. Furrer, P. Bruesch, R. Marsolais, and P. Unternahrer, Physica C **157**, 58 (1989).
[37]T. Chattopadhyay, P. J. Brown, B. C. Sales, L. A. Boatner, H. A. Mook, and H. Maletta, Ref. 31.